"ANOMALOUS EM SIGNALS AND CHANGES IN RESISTIVITY AT PARKFIELD: COLLABORATIVE RESEARCH BETWEEN THE UNIVERSITIES OF CALIFORNIA AT BERKELEY AND RIVERSIDE AND OREGON STATE UNIVERSITY"

FINAL REPORT FOR JANUARY, 2005- JANUARY, 2006
APRIL, 2007

STEPHEN PARK
University of California, Riverside
The Institute of Geophysics and Planetary Physics
Riverside, California 92521
(951)-827-4501;(951)-827-4324(fax)
magneto@ucrmt.ucr.edu

Submitted to:

UNITED STATES DEPARTMENT OF THE INTERIOR
GEOLOGICAL SURVEY
NATIONAL EARTHQUAKE HAZARDS REDUCTION PROGRAM

Grant 05HQGR0036

"ANOMALOUS EM SIGNALS AND CHANGES IN RESISTIVITY AT PARKFIELD: COLLABORATIVE RESEARCH BETWEEN THE UNIVERSITIES OF CALIFORNIA AT BERKELEY AND RIVERSIDE AND OREGON STATE UNIVERSITY"

FINAL REPORT FOR JANUARY, 2005- JANUARY, 2006
APRIL, 2007

STEPHEN PARK
University of California, Riverside
The Institute of Geophysics and Planetary Physics
Riverside, California 92521
(909)-787-4501;(909)-787-4324(fax)
magneto@ucrmt.ucr.edu

Submitted to:

UNITED STATES DEPARTMENT OF THE INTERIOR
GEOLOGICAL SURVEY
NATIONAL EARTHQUAKE HAZARDS REDUCTION PROGRAM

Grant 05HQGR0036

Abstract

The occurrence of the September 28, 2005 earthquake in Parkfield completed our electric field monitoring experiment begun in 1988. Continuous measurements of natural electrical currents (telluric currents) were made in Parkfield in order to detect relative changes of resistivity of 1% or less over both short (days) and long (years) term periods. Small changes of resistivity prior to rock failure, well documented in laboratory measurements, will rearrange the distribution of telluric currents. This rearrangment will manifest itself in changes in telluric coefficients relating electric field strength between dipoles. Unfortunately, this experiment did not record any precursory, coseismic, or postseismic changes in telluric coefficients. Our work during this period focused on providing upper bounds on the magnitude of potential resistivity changes that would still be consistent with our observations. This effort involved developing a 3D resistivity model for Parkfield and then using perturbations to it to predict how those changes would appear in the telluric coefficients. While our results are quite model-dependent, we do not think that changes in resistivity of greater than 5% along the fault could have occurred.

Introduction

Changes of electrical resistivity and anomalous electrical signals due to compression and shearing of rocks have been observed in many laboratory experiments. Field observations, although more controversial because of the magnitudes of the changes, have also reported variations of electrical resistivity. In all of these cases, fluids play a crucial role in the resistivity changes and anomalous signals because most of the electrical current in crustal rocks is transferred through conductive brines occupying the pore/fracture space of the rocks.

The results from the 2004 Parkfield earthquake were disappointing because we saw no changes in telluric coefficients, as presented in the attached manuscript. However, we used this lack of change to constrain the maximum change in resistivity that could have occurred along the fault. If the resistivity changed by more than the amount given in the manuscript (~5%), then measurable perturbations in the telluric coefficients would have been observed.

Data Availability

Time series data and processed results are available via anonymous ftp from vortex.ucr.edu (138.23.185.132) in pub/pkfld. Data from 1988-2004 are presently available. Time series data from 1998-present are also available from the Northern California Earthquake Data Center at UC Berkeley.

Conclusions

Although changes of resistivity associated with stress and strain are some of the clearest phenomena observed in the laboratory, the telluric monitoring experiment in Parkfield recorded no variations in responses prior to, during, or after the September 28, 2004 M6 earthquake there. Using the lack of observed changes, we have attempted to determine the maximum resistivity change that could have occurred and still produce no observable changes in the telluric coefficients. Such bounds are model dependent, but we used a 3-D electrical resistivtity model of the Parkfield region in order to make our calculations as accurate as possible. With this model, we estimate that no changes exceeding 5% could have occurred on the fault. Our results provide guidance for any future experiments; response parameters need to be measured with precisions of smaller than 0.1% (and preferably 0.01%) if tectonically-related resistivity changes are to be measured.

Electrical Resistivity Changes Not Observed with the 28 September 2004 M6.0 Parkfield Earthquake on the San Andreas Fault, California

Stephen K. Park, Jimmy C. Larsen
Institute of Geophysics and Planetary Physics
University of California
Riverside, CA 92521

Tien-Chang Lee
Department of Earth Sciences
University of California
Riverside, CA 92521

Abstract

An 18 year long experiment to capture changes in electrical resistivity prior to, during, and after a M6 earthquake on the San Andreas fault at Parkfield, California culminated with an event of that magnitude on 28 September 2004. Resistivity was monitored with a telluric array, giving precisions in measured parameters of 0.2% or less. No coseismic resistivity changes greater than 5% could have occurred or they would have been detected by the array, and any precursory changes would have been much smaller because maximum possible precursory strains were 4000 times smaller than the coseismic strain. Given that the earthquake ruptured directly beneath the telluric array, this experiment places a bound on the amount resistivity might change at the hypocentral location; changes measured with instruments farther from earthquakes can only be smaller. We cannot exclude the possibility that a measurable change with a larger earthquake is possible or that other fault geometries are capable of generating larger signals, but our results show clearly that future experiments should be designed with precisions of much better than 0.1% if they are to be successful.

Introduction

On 28 September 2004, the long anticipated M 6.0 Parkfield earthquake occurred [*Langbein et al.*, 2005]. Located in central California on the San Andreas fault (Figure 1), Parkfield was the site of 6 previous earthquakes in 1857, 1881, 1901, 1922, 1934, and 1966 with magnitudes of approximately M 6.0 [*Bakun and McEvilly*, 1984]. Seismograms from the last three earthquakes in the series were so similar that *Bakun and McEvilly* [1984] proposed that these events originated at the same location (circled cross in Figure 1). Further, they suggested that these earthquakes occurred regularly with a period of 22 years (actual intervals were 24, 20, 21, 12, and 32 years) and predicted that the next in the series would occur between 1988 and 1993. The Parkfield Prediction Experiment was born in the mid-1980's with the goal of recording a range of physical phenomena prior to, during, and after the next earthquake in the series [*Bakun and Lindh*, 1985]. By the early 1990's, seismometers (both at the surface and in boreholes), accelerometers, creepmeters, water well sensors, borehole strainmeters, Global Positioning System (GPS) receivers, and magnetometers had been installed in Parkfield [*Roeloffs and Langbein*, 1994]. Also, we installed the telluric array described below in order to monitor small (0.1%) changes of resistivity over scales of kilometers (Figure 1).

The earthquake on 28 September 2004 arrived long after the anticipated time of occurrence and while the prediction was therefore a failure, this M 6.0 earthquake did provide many results for the Parkfield Prediction Experiment. The hypocenter was located at a depth of 8.8 km, and the earthquake ruptured northward along the fault directly beneath the telluric array (Figure 1) before halting at Middle Mountain [*Langbein et al.*, 2005]. The earthquake was followed by two M 5 aftershocks, a number of 5 > M >

4 aftershocks, and numerous smaller events. To our knowledge, this is the closest any resistivity monitoring experiment has been to a moderate or large earthquake. While *Tank et al.* [2005] were conducting an MT survey across the fault at the time of the 1999 M7.4 Izmit earthquake, they did not report any coseismic changes of resistivity. They were also able to find a single resistivity model that was consistent with soundings recorded both before and after the earthquake, suggesting any such changes must have been small.

Because our purpose is to estimate bounds on resistivity changes that may have occurred with the 2004 Parkfield earthquake, we begin with a review of the telluric array and the precision of its measurements and then present results for 5 months spanning the earthquake. However, the array measures telluric transfer functions and not resistivity so we compare our observations to those predicted from a 3-D model that is perturbed by amounts estimated from a dislocation model for the earthquake. Because our purpose is to place an upper bound on the size of the possible resistivity change, we make some assumptions at several stages that will overestimate the effect at each stage. Basically, we try to make assumptions that maximize the possible resistivity changes and provide a most favorable interpretation of our observations. As we will show, the possible changes are still quite small.

Telluric Array

We used a telluric array measuring only electric fields because at the time of the initiation of this experiment (1987), it was the only way with passive electromagnetic measurements to obtain precisions of better than 1% in transfer functions. More

conventional magnetotelluric (MT) methods determine transfer functions between electric and magnetic fields and even today, the very best precisions are only 1% [*Eisel and Egbert*, 2001]. *Park* [1991] demonstrated that precisions approaching 0.1% were achievable with a telluric array, and this is almost an order of magnitude better than the best analysis using a magnetic reference for transfer functions. Finally, we (Park and Larsen) have tried unsuccessfully for several years to achieve precisions of 0.1% using a magnetic remote reference at Fresno; we can only reach a level of 1% using the magnetic fields.

The telluric method involves computing a transfer function between electric fields recorded at two stations simultaneously [*Berdichevsky*, 1965] and is based on the assumption that the induced magnetic fields are coherent between the two stations. The vector electric field (***E***) is linked to the vector magnetic field (***H***) by a tensor magnetotelluric (MT) transfer function, ***Z***. If $\boldsymbol{E}_1 = \boldsymbol{Z_1 H}_1$ at the first station, $\boldsymbol{E}_2 = \boldsymbol{Z_2 H}_2$ at the second station, and the magnetic fields are related through a magnetic transfer function ($\boldsymbol{H}_1 = \boldsymbol{M H}_2$), the telluric relationship can be written:

$$\boldsymbol{E}_1 = \boldsymbol{T E}_2 \tag{1}$$

where the dimensionless telluric transfer function is given by $\boldsymbol{T} = \boldsymbol{Z_1 M / Z}_2$. We make a further simplification by assuming that the electric field is uniform on the dipole, so that the voltage is just $E_l * \Delta l$, where E_l is the component of the electric field parallel to the dipole, and Δl is the dipole length. Incorporating line lengths into the telluric transfer function, we finally arrive at the equation used to analyze time varying records from the dipoles:

$$V_i(t) = x_i * V_7(t) + y_i * V_8(t), \tag{2}$$

where V_i is the time varying voltage on dipole i. Because we do not have a second station, we use dipoles 7 and 8 (constructed from Ff-Hr and Tf-Hr, respectively) as references for the other 6 dipoles (Figure 1).

Long dipoles were chosen for this array because they are relatively insensitive to variations in precipitation and temperature, as demonstrated by *Park* [1991]. Additionally, *Anzhong* [1982] showed that dipoles shorter than 1000 m experienced seasonal resistivity variations in excess of 1% and recommended that dipoles longer than 1500-3000 m be used to minimize annual changes due to precipitation and temperature.

Dipole voltages are sampled every 30 s by a 24 bit digital acquisition system after analog filtering with a lowpass of 300 s and amplification of signals by factors of 20 or 40. Dipoles are constructed by differencing signals at 5 electrodes (Figure 1) connected to a central recording location with telephone wires rented from a local telephone company. Data are archived in near real time at the Northern California Earthquake Data Center (www.ncedq.org).

Daily estimates of wideband (300-7200 s) telluric coefficients, x_i and y_i, are computed using robust processing techniques that reject outliers in the time domain [*Park*, 1991]. While coherencies between the observed voltage in (2) and the predicted one using the reference dipoles and the telluric coefficients are generally above 0.998, *Park* [1991] showed that these coefficients still varied too much (15%) due to slight rotations of the electric field direction presumably in response to source variations. *Madden* [1983] showed that projection of the change of the coefficients onto eigenvectors representing the directions of the principal axes of the field polarizations resulted in much less variation for monitoring. Essentially, small rotations of the telluric polarization

ellipse lead to systematic changes in both *x* and *y*. Projection onto average eigenvectors (see Appendix 1) for the field determined from analysis of all of 1988 reduces the variation to 1% or less [*Park*, 1991]. These projections are:

$$P1 = (x_i - \bar{x}_i, y_i - \bar{y}_i) \bullet \begin{bmatrix} V_{17} \\ V_{18} \end{bmatrix}, \quad (3)$$

and

$$P2 = (x_i - \bar{x}_i, y_i - \bar{y}_i) \bullet \begin{bmatrix} V_{27} \\ V_{28} \end{bmatrix}. \quad (4)$$

where $\overline{x_i}$ and $\overline{y_i}$ are average telluric coefficients for dipole i for all of 1988. The eigenvectors $(V_{17}\ V_{18})$ and $(V_{27}\ V_{28})$ are oriented perpendicular (3) and parallel (4) to the San Andreas fault in Parkfield, respectively. In essence, projection P1 is related to variations in the field direction perpendicular to the fault and projection P2 is related to variations parallel to the fault**.** The parallel telluric component (P2) is much more sensitive to noise because it is oriented in the direction of the minor eigenvector (see Appendix 1). While the daily variation of the perpendicular telluric component (P1) is approximately 0.1%, the daily variation of P2 is 2%. *Park* [1991; 1997] also found that a 9 day weighted running average was necessary to reduce the variability to levels less than 1%; this running average is applied to all projections presented here. Note that we use 1988 as a reference year for average coefficients and eigenvectors in order to detect any secular variations over the period 1988-2005. We will refer to the perpendicular (P1) and parallel (P2) telluric components as the major and minor telluric components, respectively.

Telluric Component Variations in 2004

Daily smoothed telluric components for Dipoles 1 through 6 for a period from late May to the end of October, 2004 show little variation either prior to, during, or after the 28 September earthquake (Figures 2 and 3). We do not present the data for the entire year here because they also show no large variations. Variations on dipoles 1, 3, 4, and 5 are generally less than 0.2% except of a period in late August when changes approached 0.5%. Dipoles 2 and 6 show greater variability with random fluctuations of 0.5% and maximum changes of 1.0% in late August (Figures 2 and 3). The larger fluctuations in late August also have larger errors and thus are less reliable. Telluric components were exceptionally stable during the month before and the month after the earthquake for all dipoles, although gaps in the time series represent days when the coherency between the measured signal and the signal predicted using the daily telluric coefficients was less than 0.998.

The variations in the telluric components for this 5 month interval are comparable to or smaller than ones seen throughout the life of the telluric array through December 2005, and none are statistically significant at the 95% confidence interval [*Park*, 1997]. All of these fluctuations are at least a factor of 5 smaller than ones that *Park* [1997] identified as possibly associated with M 4-5 earthquakes that occurred in Parkfield between 1989 and 1995. We therefore conclude that no fluctuations of the telluric components greater than 0.2% occurred prior to, during, or after the M6 earthquake.

Multiyear Changes in Telluric Components

Long term variations in components are also absent. Monthly averages of telluric components from 1990 to 2005 show even less variation than is seen in Figures 2 and 3 (Figures 4 and 5). While there appears to be a change in both telluric components on Dipole 2 after the 2004 earthquake(Figure 4), this is actually due to an instrumental problem with that channel. Because the dipoles are not real but are constructed by differencing two electrode signals, we can use the sum of the voltages around a loop to check the analog electronics [*Park*, 1997]. The sum of Dipole 5 plus Dipole 3 minus Dipole 2 should be identically zero because Lc-Tf + Tf-Hq – (Lc-Hq) all cancel; Dipoles 6, 1, and 2 have a similar relation. Loops 5-2+3 and 6-1+2 began showing deviations from zero at the beginning of 2005, and the problem is traced to Dipole 2. Thus, excluding the instrument problem with Dipole 2, none of the other dipoles showed fluctuations greater than 0.2% over the duration of the experiment.

Linking Telluric Components and Changes of Resistivity

The components discussed above are measured Earth responses to an external source field and are modulated by the local resistivity structure, although not simply. The process of relating changes in telluric components to perturbations of resistivity requires a 3-D model of resistivity and an inverse program to determine where changes are needed to simulate the component changes. Because we saw no changes in telluric components, it would seem that there were no measurable changes in resistivity. However, can we place upper bounds on the magnitude of resistivity changes that we might have *missed*?

In order to establish these bounds, we could compute the effect of a perturbed region in a homogeneous halfspace. This may lack the effects of current channeling by heterogeneous resistivity distributions, so we chose instead to construct a 3-D resistivity model based on prior work in Parkfield. We then perturb this model and use a 3-D MT modeling code [*Mackie and Madden*, 1993] with Mackie's latest proprietary improvements [Mackie, personal communication, 2006] to predict what changes in telluric components would occur. We decrease the resistivity perturbations until the predicted changes in telluric components are smaller than the variations seen in Figures 2 and 3. These scaled perturbations represent upper bounds. An important consideration is *where* to place the resistivity perturbations. We assume that a useful resistivity change must be related to the mechanical changes associated with the earthquake and use a slip estimate of the M6.0 earthquake from *Langbein et al.* [2005] in a dislocation model [*Okada*, 1972] to predict where dilatations occur and then perturb the resistivities there. This assumption is supported by many laboratory experiments [e.g., *Brace and Orange*, 1968].

We will also show the sensitivity to changes of resistivity at different depths and different positions along the rupture zone of the M6 earthquake by perturbing the 3-D resistivity model by a small percentage. These tests are similar to those presented by *Park and Fitterman* [1991] but are computed using the 3-D MT modeling code.

Deriving a 3-D Resistivity Model

The 3-D model we use here is a synthesis of others' work and that is refined where we had MT data from *Unsworth et al.* [1977] using a 3-D MT inversion [*Mackie and Madden*, 1993]. Magnetotelluric soundings have been made in the Parkfield area by

Boudreau [1989], *Park et al.* [1991], and *Unsworth et al.* [1997; 2000; 2004]. We constructed a preliminary 3-D model (Figure 6) that contained essential features of the models derived from these studies and also matched constraints from surface geology, bathymetry, and other regional geophysical studies [e.g., *Prodehl*, 1979; *Zoback and Wentworth*, 1986; proprietary well log data]. This 3-D model contains multiple scales and extends to 6000 km in all directions from Parkfield. Such large distances are needed in order to correctly model the coast effect from the nearby Pacific Ocean [see *Park et al.* 1991 for details]. We then attempted to refine this model with 3-D inversion. The changes in resistivity structure in response to fitting Unsworth's data occurred to the north of the array where the MT sites were located and the model under all but the northernmost part of the array was unchanged. Thus, the tests here involve perturbing the portions of the model that were assembled from older, 2-D models of the region and further discussion of the 3-D inversion is unnecessary here**.** New data from an MT survey in Parkfield [*Becken et al.*, 2005] may become available in the future and we can refine our model with these data at that time. However, that survey is also focused mostly to the north of the array where we already have constraints from earlier surveys and is unlikely to affect our model beneath the array. We also attempted to combine our 3-D model with the earlier one from *Park and Fitterman* [1990], but forward modeling with this composite model led to greater errors in fits to the MT data and we ultimately did not use their results (Note that their model was derived for dc resistivity data using trial-and-error forward modeling, so the misfit with the MT data may not be surprising.)

Perturbing the Resistivity Model

The M6 earthquake in Parkfield ruptured a region approximately 20 km long that extends from the surface to a depth of 11 km [*Langbein et al.*, 2005]. The earthquake initiated at base of the rupture patch and 3 km south of our electrode at Hr and then propagated northward beneath our array before terminating just north of Dipole 6 (Figure 1). Slip was complex with one locus centered on the hypocenter at 9 km and a second one centered beneath Dipole 6 (Figure 1) at a depth of 7 km [*Langbein et al.*, 2005]. Our array was thus centered over the slip plane and ideally placed to maximize responses from changes in resistivity.

Because our goal is to estimate changes in resistivity and not examine the details of the fault plane, we simplify the slip model of *Langbein et al.* [2005] to a plane 20 km long extending from the surface to 9 km depth with a uniform slip (Figure 1). Using the moment magnitude of 10^{18} Nm [*Langbein et al.*, 2005] and a shear modulus of $3X10^{10}$ N/m^2, we compute the uniform slip on this plane of 0.18 m. This is comparable to the average slip of 0.155 m computed by *Langbein et al.* [2005] from static GPS and waveform data. Dilatations predicted using a dislocation model [*Okada*, 1992] with uniform slip of 0.18 m on a patch 20 km long and 9 km deep are concentrated at the ends of the patch, near the northern and southern extent of the telluric array (Figure 7). Maximum volumetric strains of 40 microstrains ($\Delta V/V = 40x10^{-6}$) are predicted with compressions occurring in the northwest and southeast quadrants and expansions occurring in the southwest and northeast quadrants, as expected from right lateral shear on the fault (Figure 7).

The dislocation model gives us the locations of possible resistivity changes, but we still need to estimate their sizes. Laboratory data show that rocks exhibit large variations in their responses to stress and strain because of lithologic differences and degree of fracturing [e.g. *Brace et al.*, 1965; *Yamazaki*, 1968; *Brace and Orange*, 1968; *Fitterman*, 1975; *Morrow and Brace*, 1981]. Typically, sensitivities are expressed in terms of %change/bar ($[\Delta\rho/\rho]/\Delta P$) or %change/%strain ($([\Delta\rho/\rho]/[\Delta\varepsilon/\varepsilon]$) where ρ is resistivity and $\Delta\varepsilon/\varepsilon$ is strain. Because we have computed dilatations, we use strain sensitivity here. Strain sensitivities range from less than 100 to over 1000 for saturated tuffs [*Yamazaki*, 1968] and are much larger (10^5) if the tuffs are partially saturated [*Morrow and Brace*, 1981]. Other rocks show lower sensitivities [*Brace and Orange*, 1965]. Because our goal is to provide an *upper* bound on the magnitude of the resistivity changes, we scale the dilatations by a factor of 1000 to estimate ±2% changes that may have occurred at the surface and as much as ±4% at depth. We then perturb the resistivity model (Figure 6) by these amounts at the locations shown in Figure 7; while magnitudes varied at different depths, the overall pattern in each layer is similar to that at the surface. Perturbations of as much as ±2% between depths of 0-2 km, ±4% between depths of 2-6 km, and ±3% at depths of 6-11 km were applied. Because presenting the entire 3-D model and its perturbations would be difficult to present , we use instead the total change in conductance for comparisons between models. For the model perturbed by the dilatations in Figure 7 scaled by a factor of 1000, the total change in conductance is 3.18×10^8 S-m^2 (conductivity change times volume) over a volume of 1.7×10^{11} m^3. Note that the net change is calculated so that positive and negative changes do not cancel.

We also ran a series of models in which the conductivity along the San Andreas fault was increased at various locations and depths in order to simulate possible responses to enhanced permeability of fluids due to rupturing. A total of 12 regions were perturbed, with locations along the northern, central, and southern segments of the rupture zone (Figure 6). For each segment, conductivities at depths ranging from 1 to 9 km were increased by 5% (Table 1). For each segment and depth range in Table 1, responses from a separate 3-D model were computed and compared to those from the background model in Figure 6. Variability in the total conductance change between the different test models resulted primarily from the background conductivity of the perturbed region and secondarily from slight differences in volume of the perturbed region (Table 1). However, all of the models tested in Table 1 had total conductance changes much smaller than the model based on static stress changes.

Relating MT Responses to Telluric Components

We use the 3-D MT modeling algorithm of *Mackie and Madden* [1993] to compute electric fields for both the original and the perturbed models discussed in the previous section and then compare differences in the telluric components from each. However, the analysis outlined in (2)-(4) is performed with measured voltages on the dipoles (Figure 1) and results in real telluric coefficients, x and y. The MT modeling algorithm generates electric fields by simulating the process of electromagnetic (EM) induction at low frequencies, so we must relate these electric fields to our measured telluric components. There are actually three problems in linking measured voltages and calculated fields (Appendix 2). First, the dipole measures a voltage and the model

generates electric fields, so we must integrate the electric fields between the endpoints of the dipole in order to get the voltage. Second, the telluric components (P1, P2) are determined from average telluric coefficients (x, y) for a band spanning 300-7200 s periods and the MT model computes responses at discrete periods. We show in Appendix 2 that the wideband average for our model is equivalent to the value at a period of 1550 s, so the comparisons shown are done only for this period. Note that we can average these long period responses because the skin depth at the shortest period of 300 s with a resistivity of 60 ohm-m is ~60 km while we are perturbing the resistivity only in the upper 10 km. Thus, the region of resistivity change is a thin layer and its effect is primarily to scale electric field amplitudes (the MT 'static shift'; e.g., *Jones* [1988]). Third, EM induction results in phase shifts between electric fields at different points and the telluric analysis assumes no phase shifts. We show in Appendix 2 that while there are phase shifts in the computed responses, they are small.

In order to simulate coseismic changes in telluric components, we subtract the telluric components before the resistivity perturbation from those after the perturbations. The magnitude of each component change depends on the orientation of the dipole, the location of the dipole relative to the volume where the resistivity changed, and the interaction between that volume and adjacent model elements. Because the perturbed volume is embedded in a much larger volume that experiences no change and because electromagnetic induction at long periods averages over large volumes of crust, the effect of this volume is typically diluted. Changes in telluric components will usually be smaller than the perturbations in resistivity, but may be larger if there are focusing effects from the structure [*Park and Fitterman*, 1990].

While the longer dipoles effectively minimize variations from precipitation and temperature, they can also have the effect of averaging out variations of resistivity. Small scale changes associated with earthquake or premonitory processes could be missed. We will show that the perturbed models tested here *still* produce changes in telluric components that would have been measurable with the longer dipoles. We cannot exclude the possibility that we may have missed smaller scale changes that could have been detected with shorter dipoles but suggest that such small changes would likely have been missed in the environmental 'noise' from variations in precipitation and temperature.

The model with up to 4% changes in resistivity due to dilatation generates maximum changes in telluric components of only 0.13% on Dipole 6; all other changes were below 0.10% (Table 2). For each dipole, we present the estimated magnitude for the major and minor telluric components presented in Figures 2 and 3. This maximum change is just above the most optimistic estimate of our noise levels, so it is possible that a resistivity change in response to the static stress change could have been missed. Results from tests of individual changes along portions of the fault zone are much more encouraging, however.

Conductivity increases of 5% at various locations and depths along the San Andreas fault produced variable changes in telluric coefficients (Table 2). Changes often exceeded 0.1% and peaked with changes larger than 1% for two of the regions (Table 2). Additionally, no simple generalizations could be made about where the sensitivity was greatest. Contrary to expectations, conductivity increases in the upper 1 to 2 km along the northern portion of the fault (Figure 6) produced changes of as much as 0.73% in

Dipole 5 (Table 2); similar increases at the same depth range along the central and southern portions produced much smaller changes. Given that the northern portion of the fault had the smallest net conductance increase of any of the three regions at 1 to 2 km depths (Table 1), the relatively larger sensitivity must be related to the geometry of the array relative to the perturbed region.

Conductivity increases at intermediate depths (2 to 4 km and 4 to 6 km) also produced variable results. The largest change in telluric coefficients (1.57%) occurred on Dipole 5 in response to a conductivity increase at depths of 2-4 km beneath the northern portion of the fault (Table 2). Changes in response to conductivity perturbations at similar depths beneath the central and southern portions of the fault were much smaller (Table 2). Given that many of the regions in the intermediate depth range had similar conductance increases (Table 1), the geometry of the array must affect its response to different portions of the fault. Changes of 0.5% or greater resulted from conductivity perturbations at depth ranges of 4 to 6 km beneath the northern and central portions of the fault (Table 2), but not from the southern portion of the fault.

We had expected that the array would exhibit little sensitivity to changes in depths of 6 to 9 km because previous work by *Park and Fitterman* [1990] showed the loss of sensitivity at greater depths and because the conductance increases for the three portions at these depths were almost 10 times smaller than those at shallower levels (Table 1). Nonetheless, conductivity increases at depths of 6 to 9 km beneath the central portion of the fault resulted in coefficient changes exceeding 1% on Dipole 5 (Table 2). While changes from the southern portions of the fault were uniformly small, conductivity

increases at depths of 6 to 9 km resulted in coefficient changes exceeding 0.1% for Dipole 5 (Table 2).

Despite great variability in the sensitivity to different regions of the fault zone, it is clear that the telluric array is capable of detecting resistivity changes exceeding a few percent along the fault at depths ranging from 1 to 9 km. The sensitivity is a complex combination of the resistivity structure of the region, the location and size of the conductivity increase (or decrease), and the array geometry. A puzzling result is that the static stress model with a total conductance perturbation much larger than any of those in Table 1 did not produce large changes in telluric components. We speculate that this is because the conductivity perturbations from the static stress model were distributed over a broad region with dimensions comparable to the array. Their effects may have led to more uniform changes in voltages on all dipoles and thus smaller changes in telluric components.

Discussion

Many previous experiments report resistivity changes of several percent prior to both small and large earthquakes [e.g., *Mazzella and Morrison*, 1974; *Qian et al.*, 1983], while other high precision experiments over shorter distances observe changes not exceeding 0.01% associated with small earthquakes and creep [e.g., *Yamazaki*, 1974; *Fitterman and Madden*, 1977]. We interpreted changes in telluric components from Parkfield as evidence of resistivity perturbations [*Park*, 2002] but also showed that such changes could be statistically insignificant [*Park*, 1997]. From 1988-2004, no

earthquake larger than M5 occurred in Parkfield, so our equivocal results could have been due to lack of sensitivity to changes from small earthquakes.

The M6 earthquake in Parkfield eliminates much of the uncertainty about past fluctuations in the telluric components. The lack of fluctuations greater than 0.2% associated with the M6 earthquake constrains the possible resistivity perturbations to less than a few percent and we suggest that changes in excess of 5% reported in other experiments including our own are likely due to causes other than tectonic changes prior to small and moderate earthquakes.

This upper bound is significant for two reasons. First, our array is the closest any experiment has been to the source of a M≥6 earthquake. This proximity means that the effects of resistivity changes at the earthquake source are maximal for our array and observations made at greater distances will be necessarily smaller. This conclusion assumes that the resistivity changes are related to changes in strain and/or stress in the earthquake cycle (if they are not, then the utility of resistivity for earthquake prediction is questionable). Second, other Parkfield experiments provided estimates of the ratio of precursory versus coseismic strain. While coseismic strains of ~40 με were calculated from the slip model, maximum recorded preseismic strains were 10 nε in the months prior to the earthquake [*Langbein et al.*, 2005]. Thus, maximum preseismic changes of resistivity would be 4000 times smaller than the coseismic ones, or 0.001% maximum. No current measurement technique other than the array described by *Yamazaki* [1974] can come close to this necessary precision.

The rocks in the upper kilometer at Parkfield are relatively conductive (<60 ohm m), so it is possible that these rocks reduce the sensitivity at the surface to changes at

hypocentral depths. However, our model (Figure 6) is conductive and we still demonstrated that resistivity perturbations of 1-4% at depths up to 9 km can produce measurable changes in the telluric components at the surface. We therefore conclude that while near-surface dilution of the signal is certainly occurring, it is not sufficient to mask small resistivity changes.

We cannot exclude the possibility that earthquakes larger than M6 could still cause measurable resistivity changes with surface arrays. However, such earthquakes are even less frequent than the Parkfield earthquake and the chance of installing a monitoring array above a future hypocenter to observe precursory changes is small.

These results pose a challenge to other experiments designed to monitor electromagnetic changes prior to earthquakes. Resistivity changes will likely be much smaller than 1%, requiring measurement precision better than 0.1% in amplitude. Given that current MT processing techniques can at best provide precisions of 1% [*Eisel and Egbert*, 2001], it is unlikely that MT stations for monitoring will be useful without substantial advances in data analysis techniques.

If resistivity changes associated with major earthquakes are likely to be small or even nonexistent, then why are fault zones often conductive and when did they become so? Many recent MT studies have revealed that fault zones are conductive [e.g., *Mackie et a.l*, 1997a; *Unsworth et al.*, 2000; *Becken et al*., 2005; *Tank et al.*, 2005]. A common explanation is the presence of fluids in fractured rock on the fault. If so, then either the enhanced conductivity has developed as a consequence of many repeated events or it developed as the result of the initial fracturing and has been a feature of the fault zone since its inception. If the former, than monitoring of fault zone resistivity may eventually

result in observations of precursory changes. If the latter, then it is unlikely that monitoring will be productive. One encouraging result is the observation of *Mackie et al.* [1997b] that the locked portion of the San Andreas fault at Carrizo Plain is *not* conductive. This may indicate that enhanced conductivity is not a universal feature of active fault zones and monitoring has some promise.

Conclusions

The 2004 M6 earthquake at Parkfield, California closed a chapter in earthquake monitoring spanning almost two decades. Results from a telluric monitoring array straddling the slip region of the fault show no measurable coseismic resistivity changes larger than 5%. Given that precursory changes are likely to be much smaller, it is unlikely that monitoring resistivity changes in large volumes (~few km^3) of the crust will yield useful predictions. We cannot exclude the possibility that measurable changes will occur with M≥6 earthquakes however, or with faults in different tectonic regimes. Nonetheless, we recommend that any future resistivity monitoring experiments with any technique (MT, tellurics, dc resistivity, electromagnetics) be designed with precisions of much better than 0.01%.

This precision will be difficult to achieve with current methods and processing. Monitoring based on the magnetotelluric method is unlikely to ever reach this level unless new ways are developed of estimating transfer functions in the presence of variable source polarizations. While short dipoles in telluric arrays may be preferable, methods to separate potential tectonic signals from environmental ones have yet to be developed. Measurement of electric fields with electrodes in boreholes may eliminate the influence of surface environmental factors but may be affected by a seasonally

fluctuating water table. Future experiments should use separate sensors for each dipole so that electrode noise can be identified and rejected; we were unable to do so because of the limited availability of telephone lines.

Appendix 1

The linear relationship between the voltages on a dipole and the two reference dipoles (2) can be reformulated as a matrix equation to solve for x and y using all of the time samples for one day [*Park*, 1991]:

$$\begin{bmatrix} \boldsymbol{D_7(t)} & \boldsymbol{D_8(t)} \end{bmatrix} \begin{bmatrix} x \\ y \end{bmatrix} = \begin{bmatrix} \boldsymbol{D_i(t)} \end{bmatrix}, \qquad \text{(A1)}$$

where the left hand side is a 2880 X 2 matrix multiplying a 2 X 1 vector and the right hand side is a 2880 X 1 vector. The telluric coefficients consist of a large stable component ($\bar{x}$ $\bar{y}$) due to the average response to the mean resistivity structure and a smaller fluctuating component (Δx Δy) due to variations of resistivity, noise, and changes in source polarization. We solve directly for the fluctuating component:

$$\begin{bmatrix} \boldsymbol{D_7(t)} & \boldsymbol{D_8(t)} \end{bmatrix} \begin{bmatrix} \Delta x \\ \Delta y \end{bmatrix} = \begin{bmatrix} \boldsymbol{D_i(t)} \end{bmatrix} - \begin{bmatrix} \boldsymbol{D_7(t)} & \boldsymbol{D_8(t)} \end{bmatrix} \begin{bmatrix} \bar{x} \\ \bar{y} \end{bmatrix}. \qquad \text{(A2)}$$

The 2880 X 2 matrix formed by the time series of the reference dipoles can be decomposed into eigenvectors and eigenvalues [Lanczos, 1961]:

$$\begin{bmatrix} \boldsymbol{D_7(t)} & \boldsymbol{D_8(T)} \end{bmatrix} = \begin{bmatrix} \boldsymbol{U_1(t)} & \boldsymbol{U_2(t)} \end{bmatrix} \begin{bmatrix} \boldsymbol{\lambda_1} & \boldsymbol{0} \\ \boldsymbol{0} & \boldsymbol{\lambda_2} \end{bmatrix} \begin{bmatrix} \boldsymbol{V_{17}} & \boldsymbol{V_{18}} \\ \boldsymbol{V_{27}} & \boldsymbol{V_{28}} \end{bmatrix}, \qquad \text{(A3)}$$

where $\boldsymbol{U_i(t)}$ is an eigenvector in time series space, λ_i is an eigenvalue, and (V_{i7} V_{i8}) is an eigenvector in telluric coefficient space [*Madden*, 1983; *Park*, 1991]. The eigenvectors in telluric coefficient space define the principal axes of the electric field polarization set by the local resistivity structure. At Parkfield, the major eigenvalue is 6 times larger than

is the minor eigenvalue, so the telluric field is strongly polarized. While eigenvectors for the major eigenvalue are estimated well, those for the minor eigenvector are often more variable because the analysis tends to push the noise into this component.

Appendix 2

The dipoles in Figure 1 measure an integrated voltage given by:

$$V_i = \int_{Lk} \overline{E} \bullet \overline{dl} \qquad \text{(A4)}$$

where L_k is the path given by the kth dipole geometry. However, we use gridded 3-D models in which the dipoles span multiple blocks (Figure 6) in order to simulate the measured voltages. We must develop a method of integrating the electric fields from the grid cells to get the voltages. A simple approach is to assume that the field is constant within each grid cell and then sum the product of the electric fields and cell lengths, but this has two problems. First, the dipoles have arbitrary paths and integration of (A4) is thus difficult. Second, this simple approach assumes that the field is constant within each cell.

We solve the first problem by using an equivalent path parallel to model coordinates to compute the voltage:

$$V_i = \int_{Lx} E_x dx + \int_{Ly} E_y dy, \qquad \text{(A5)}$$

where Lx and Ly are path components in the x and y directions, respectively (Figure A1). Between two dipole endpoints, there are multiple paths and we use consistency between the results for different paths to assess validity of this approach. An additional complication with the use of different paths is that because we are modeling electromagnetic induction, the integral of the electric field over a closed loop is nonzero:

$$\oint E \bullet \overline{dl} = \int j\omega\mu \overline{H_z} dA, \qquad \text{(A6)}$$

where A is the area enclosed by the loop. Because the modeling program also computes the vertical magnetic field, we can estimate the contribution from the right hand side of (A6). For a period of 1550 s, this contribution is never greater than 0.01% of the summed voltage from (A5) and we conclude that it is negligible. *Park* [1997] computes the sum of the voltages around each of 5 loops constructed from the dipoles and finds that the voltage is only nonzero if there is a malfunction; this would suggest that field results confirm that the contribution from the vertical magnetic flux is negligible.

The more serious problem is that the fields vary within a grid cell and the integrals in (A5) have contributions from that varying field. *Poll et al.* [1989] proposed one such method for a 2-D model that predicted fields at cell boundaries. Their method used continuity of normal current density at the cell boundaries to determine the variation of the electric field perpendicular to strike within one grid cell. The field parallel to strike does not vary in a 2-D model, so an assumption of constant field in (A5) is justified. Unfortunately, this method was developed for 2-D models and fields computed at cell edges. We are modeling fields at cell centers [*Mackie and Madden*, 1993] for 3-D models, so we cannot simply use Poll et al.'s method. However, we attempted to estimate the variation of the field by assuming that the normal current density varied linearly across a block, was continuous across the boundaries, and matched the value computed at the center of each block. This effectively approximates the electric field with the first two terms of a Taylor series expansion, as opposed to the first three terms used by *Poll et al.* [1989]. We also attempted to assume that the field was locally 2-D

and use a variant of Poll et al.'s method modified for fields computed at block centers; this variant used the first three terms of the Taylor series expansion.

Our criterion for evaluating the accuracy of our estimated voltages was to compare (A5) along two paths, one of which integrated along the x direction first and then along the y direction and the other integrated along the y direction first and then along the x direction (Figure A1). Because the contribution from the vertical magnetic flux is negligible, differences between these two path integrals will be due to the assumptions made about the variation of the electric field. We began by integrating along the two paths assuming the fields were constant across each cell. Voltages differed by less than 1% for over 60% of the paths (two paths for each of two source polarizations for 8 dipoles), by over 5% for only 15% of them, and for a maximum of 10% for only one path. This would suggest that the corrections needed to account for variable electric field within a grid cell are small. Corrections were judged beneficial if they reduced the voltage differences between the two paths compared to the calculations assuming constant electric field in each grid cell.

Our corrections using the first two terms of the Taylor series expansion (thus allowing for a linear variation of the electric field across the grid cell) led to improvements for a few of the path integrations and degradations for most. In other words, adding in a correction for a linear change of electric field across a grid cell increased the differences between the two paths for all but two of the dipoles. We concluded that this correction was not helpful. The correction based on a variant of Poll et al.'s method also did not reduce differences between paths significantly. We conclude that path differences are the result either of the inadequacy of these corrections to deal

with 3-D field variations or a consequence of the approximation of derivatives with finite differences in the 3-D modeling program. In either case, further refinement is beyond the scope of this paper.

Given no better alternative, we choose to use the mean of the voltages computed by integrating the electric fields along the two paths in Figure A1 assuming that the electric field is constant within each grid cell. These voltages will be used to compute telluric transfer functions below, but our final task is to estimate changes between two transfer functions. While we cannot prove it because we do not have path-independent voltages, we assume that the errors due to approximations in (A5) will be similar for the two transfer functions because the conductivity changes and therefore changes in electric fields will be small and because the paths used will be the same.

The modeling program computes responses for two orthogonal source directions. Each solution results in one set of voltages, but each dipole has two telluric coefficients. To overcome the problem of one equation (2) with two unknown telluric coefficients, we solve the following equations for x and y:

$$V'_i(t) = x_i * V'_7(t) + y_i * V'_8(t), \tag{A7}$$

$$V''_i(t) = x_i * V''_7(t) + y_i * V''_8(t), \tag{A8}$$

where the prime and double prime voltages are the mean values of the voltages along two paths (Figure A1) for each source polarization. Telluric components are computed by taking the inner product between the changes in telluric coefficients and the eigenvectors from *Park* [1997]. The major eigenvector is oriented parallel to Dipole 8 and the minor eigenvector is parallel to Dipole 7 (Figure 1), so P1 is the component perpendicular to the fault and P2 is the component parallel to the fault.

The second concern is that the modeling program computes responses at single frequencies, but our telluric coefficients are estimated using a wide band average from 300-7200 s. We show in Table A1 the coefficients for the model in Figure 6 for periods from 334-7200 s compared to their averages. The coefficients at a period of 1550 s are comparable to the averages, so we used values at this period for comparisons between models with and without perturbed resistivities.

Finally, EM induction introduces phase shifts that are ignored in our robust analysis for telluric coefficients. However, the tests in Table A1 also examine these phase shifts because the phase is related through a Hilbert transform to the change in amplitude with period. While this result was first derived for the magnetotelluric impedance [*Boehl et al.*, 1977], recognition of the telluric transfer function as a ratio of two magnetotelluric impedances leads to the conclusion that the phase in the telluric transfer function should be related to the logarithmic derivative of the amplitude curve with respect to period. For Dipole 2 (Table A1), the change in amplitude for the y component predicts a phase of 6.7º. A computed phase shift of 7.2º for this component is very close to that expected from the slope of the amplitude curve, thus confirming the phase-amplitude relationship. Note that all other telluric transfer function coefficients showed much less variation with period and their phases (not shown) are correspondingly small ($< 1^{o}$).

The variation in amplitude with period is observed only in the model; the array data show no such variations or phases [Park, 1997]. Analysis of band limited data in three bands centered at 424 s, 1468 s, and 5134 s showed that the telluric coefficients for the lower two bands were within 0.01% of one another for all dipoles. Larger variations

and lower coherencies were seen in the highest band (424 s) because of smaller signal levels and the effect of filtering with a two pole low pass filter rolling off at periods less than 300 s [Park, 1997]. We conclude that phase shifts affect our data only at levels below the sensitivity of the array (0.1%) and can thus be ignored.

Acknowledgements

We would like to dedicate this work to Ted Madden, a mentor whose ideas are embodied in the telluric array method. Many people worked on this project over its 18 years and are mentioned in previous publications. More recently, we thank Amy Basso, Will Dalrymple, and Randy Mackie for assistance with the array operations and 3-D modeling. Robert Simpson kindly gave us his dislocation modeling programs based on *Otada* [1992]. Reviews by Alan Jones (athough often painful!), Andreas Junge, and two anonymous reviewers were very helpful. This work was supported by the U.S. Geological Survey (USGS), Department of the Interior, under USGS Award numbers 05HQGHR0036. The views and conclusions contained in this document are those of the authors and should not be interpreted as necessarily representing the official policies, either expressed or implied, of the U.S. Government. Seismic data are from the Northern California Earthquake Data Center operated by the Berkeley Seismological Laboratory.

Figure Captions

Figure 1 – Telluric array in Parkfield, California. Dipoles 1-8 are virtual dipoles constructed by differencing voltages measured at 5 electrodes Ff, Hr, Hq, Lc, and Tf. The focal mechanism diagram of main shock and locations of aftershocks are shown.

Aftershocks less than M5 are scaled by magnitude, with the smaller ones as filled circles and the larger ones as open circles. The two M5 aftershocks are shown in the northwest corner of the map with filled circles to make them more visible, however. Shaded quadrilateral in middle shows slip plane used in dislocation modeling. The circled cross immediately north of Dipole 5 denotes the epicenter of 1966 M6 Parkfield earthquake.

Figure 2 – Telluric components for Dipoles 1, 2, and 3 from May-October, 2004. For each dipole, the major component (P1), minor component (P2), and the multiple coherency between observed signal and that predicted from daily telluric coefficients (x,y) are shown. A coherency of 1.0 means perfect correlation; lower numbers indicate data with noise. Days with coherencies of less than 0.998 are rejected in analysis. Telluric components are smoothed with a 9 day weighted running average, and the light error bars represent 95% confidence intervals. Shaded region at end of September denotes time of main shock and two M5 aftershocks. On each right side of each plot, the error bar in bold shows the size in percent of the maximum variation for any of the models tested. Maximum variations of less than 0.1% are not shown, however. Note that the predicted variations exceed the fluctuations of the telluric components for Dipoles 2 and 3 during the month prior to the earthquake.

Figure 3 – Telluric components for dipoles 4, 5, and 6 for May- October, 2004. See caption of Figure 2 for explanation. Variations predicted from the model exceed fluctuations of the telluric components for Dipole 5.

Figure 4 – Long term fluctuations in telluric components for dipoles 1, 2, and 3 from 1990-2005. See caption of Figure 2 for explanation. Variations in shaded area in 2005 on Dipole 2 are due to instrumental problems. Time of M6 earthquake is shown by arrow.

Figure 5 – Long term fluctuations in telluric components for dipoles 4, 5, and 6 from 1990-2005. See captions of Figures 2 and 4 for explanation.

Figure 6 – A)Top layer (0-30 m) of 3-D resistivity model determined from MT data and used for base model in computations. Perturbations of up to 4% or 0.4% at depths up to 11 km were made using the dilatation model in Figure 7 to predict where to make changes. Three lines of squares show locations of MT soundings from *Unsworth et al.* [1997;2000]. White boxes labeled N, C, and S indicate map views of the northern, central, and southern regions along the San Andreas Fault that were used to determine the telluric array's sensitivity to resistivity changes (see text for discussion). Dashed line A-A' is location of cross section in Figure 6b. B) Cross section through 3-D resistivity model along A-A'. Locations of the San Andreas Fault (SAF) and electrode Lc are shown. Vertical and horizontal scales are equal. White boxes show depth ranges for resistivity blocks perturbed in each of the northern, central, and southern regions.

Figure 7 – Dilatations predicted from slip on shaded plane for main shock in Parkfield on 28 September 2004. Dilatations are concentrated at ends of slip plane and locally approach 40 microstrains (με). The pattern of dilatation (positive) and compression

(negative) is consistent with right lateral strike slip motion on fault. Inset box represents extent of dislocation model volume.

Figure A1 – Example of two integration paths for computation of voltage between ends of dipoles. Path 1 integrates along x first and then y; path 2 reverses this order. Ideally, both integrals should result in the same voltage for the dipole.

Tables

Table 1 – Parameters of Models Testing Enhanced Conductivity along the Rupture Zone

Model	Segment	Area, km^2	Depth Range, km	Conductance, $S \bullet m^2$
A1	N	1.1 km X 7 km	1-2 km	3.4×10^7
A2	N	1.1 km X 7 km	2-4 km	4.1×10^7
A3	N	1.1 km X 7 km	4-6 km	6.9×10^7
A4	N	1.1 km X 7 km	6-9 km	6.8×10^6
B1	C	1.1 km X 7.5 km	1-2 km	8.7×10^7
B2	C	1.1 km X 7.5 km	2-4 km	3.9×10^7
B3	C	1.1 km X 7.5 km	4-6 km	4.2×10^7
B4	C	1.1 km X 7.5 km	6-9 km	3.3×10^6
C1	S	1.1 km X 5.5 km	1-2 km	7.4×10^7
C2	S	1.1 km X 5.5 km	2-4 km	2.7×10^7
C3	S	1.1 km X 5.5 km	4-6 km	2.4×10^7
C4	S	1.1 km X 5.5 km	6-9 km	2.5×10^6

Table 2 – Percent Changes in Projections Exceeding 0.1% for Test Models

Model		Ff-Hq(1)		Lc-Hq		Tf-Hq		Hr-Hq		Lc-Tf		Ff-Lc	
Depth	Zone	P1	P2	P1	P2	P1	P2	P1	P2	P1	P2	P1	P2
1-2	N	-	-	-	+0.13	+0.15	-0.17	-	-	**-0.64**	**-0.73**	-0.16	+0.17
km	C	-	-	-	-	-	-	-	-	-	-0.10	-	-
	S	-	-	-	-	-	-	-	-	-0.20	+0.22	-0.11	+0.13
2-4	N	-	-	+0.36	-0.41	-0.29	+0.32	-0.14	+0.16	**+1.45**	**-1.57**	-	+0.11
km	C	-	-	+0.13	+0.20	+0.25	-0.22	+0.14	-0.10	**-0.86**	**+0.93**	-	-
	S	-	-	-	-	-	-	-	-	-	-	-	-
4-6	N	-	-	+0.15	-0.19	-0.10	+0.14	-	-	**+0.59**	**-0.73**	-0.13	+0.14
km	C	-	-	-	+0.11	+0.13	-0.14	-	-	-0.48	**+0.54**	-	-
	S	-	-	-	-	-	-	-	-	-	-	-	
6-9	N	-	-	-	-	-	-	-	-	-0.10	-0.18	-	-
km	C	- 0.10	+0.11	-0.20	+0.23	+0.26	-0.29	-	-	**-1.04**	**+1.11**	-0.13	+0.14
	S	-	-	-	-	-	-	-	-	+0.11	-0.13	-	-
Strain Model		-	-	-	-	-	-	-	-	-	-	-0.11	+0.13

Table A1 – Comparison of Wide Band Averages to Individual Periods

Dipole	T, sec	7200	3342	1550	720	334	AVE
1	x	-.7340	-.7327	**-.7323**	-.7303	-.7267	**-.7312**
	y	-.3163	-.3147	**-.3140**	-.3117	-.3078	**-.3129**
2	x	-.4600	-.4529	**-.4510**	-.4502	-.4442	**-.4517**
	y	0.0462	0.0537	**0.0557**	0.0568	0.0638	**0.0553**
3	x	0.2934	0.2934	**0.2963**	0.3020	0.3020	**0.2974**
	y	0.7417	0.7414	**0.7436**	0.7491	0.7492	**0.7450**
4	x	0.2574	0.2604	**0.2622**	0.2641	0.2669	**0.2622**
	y	-.2612	-.2582	**-.2565**	-.2545	-.2515	**-.2564**
5	x	-.7682	-.7536	**-.7561**	-.7655	-.7564	**-.7600**
	y	-.6998	-.6839	**-.6852**	-.6941	-.6838	**-.6894**
6	x	-.2746	-.2764	**-.2785**	-.2804	-.2816	**-.2783**
	y	-.3487	-.3503	**-.3519**	-.3539	-.3558	**-.3521**

References

Anzhong, J., A method is given for finding the steady normal variation of earth resistivity at the zone of high-resistivity screening layer near surface, *Acta Geophys. Sinica, 25*, 193-197, 1982.

Bakun, W.H., and A.G. Lindh, The Parkfield, California earthquake prediction experiment, *Science, 229*, 619-624, 1985.

Bakun, W.H., and T.V. McEvilly, Recurrence models and Parkfield, California, earthquakes, *J. Geophys. Res., 89*, 3051-3058, 1984.

Becken , M., O. Ritter, S. Park, and M. Weber, Imaging the deep roots of the San Andreas fault zone with magnetotelluric measurements, *EOS Trans. Am. Geophys. Union 86(52)*, Fall Meet. Suppl., Abstract T23E-06, 2005.

Berdichevskii, M.N., Electrical prospecting with the telluric method, transl. by G.V. Keller, *Q. Colo. Sch. Mines, 60*, 216 pp., 1965.

Boudreau, P., A magnetotelluric and D.C. resistivity survey near Parkfield, California, MS Thesis, University of California, Riverside, California, 1989.

Brace, W.F., and A.S. Orange, Electrical resistivity changes in saturated rocks during fracture and frictional sliding, *J. Geophys. Res., 73*, 1433-1445, 1968.

Brace, W.F., A.S. Orange, and T.R. Madden, The effect of pressure on the electircal resistivity of water-saturated crystalline rocks, *J. Geophys. Res., 70*, 5669-5678, 1965.

Eisel, M., and G.D. Egbert, On the stability of magnetotelluric transfer function estimates and the reliability of their variances, *Geophys. J. Int.*, 144, 65-82, 2001.

Fitterman, D.V., Electrical conductivity of compressed kaolinite (abstract), *Eos Trans. Am. Geophys. Union, 56*, 1068, 1975.

Fitterman, D.V., and T.R. Madden, Resistivity observations during creep events at Melendy Ranch, California, *J. Geophys. Res., 82*, 5401-5408, 1977.

Jones, A.G., Static shift in magnetotelluric data and its removal in a sedimentary basin environment, *Geophys., 53*, 967-978, 1988.

Langbein, J., R. Borcherdt, D. Dreger, J. Fletcher, J.L. Hardebeck, M. Hellweg, C. Ji, M. Johnston, J.R. Murray, R. Nadeau, M.J. Rymer, and J.A. Teriman, Preliminary report on the 28 September 2004, M6.0 Parkfield, California earthquake, *Seis. Res. Lttr., 76*, 10-26, 2005.

Mackie, R.L., and T.R. Madden, Three-dimensional magnetotelluric inversion using conjugate gradients, *Geophys. J. Intl., 115*, 215-229, 1993.

Mackie, R.L., T.R. Madden, and E.A. Nichols, A magnetotelluric survey of the Loma Prieta earthquake area: implication for earthquake processes and lower crustal conductivity, *in* Reasonberg, P.A. (ed.), *Loma Prieta, California, earthquake of October 17, 1989: aftershocks and postseismic effects*, U.S. Geol. Surv. Prof. Pap., U.S. Geol. Surv., Reston, Virginia, D289-D312, 1997a.

Mackie, R.L., D.L. Livelybrooks, T.R. Madden, and J.C. Larsen, A magnetotelluric investigation of the San Andreas fault at Carrizo Plain, California, *Geophys. Res. Lett., 24*, 1847-1850, 1997b.

Madden, T.R., High sensitivity monitoring of resistivity and self-potential variations in the Palmdale and Hollister areas for earthquake prediction studies, final technical report, U.S. Geol. Surv. project 14-08-0001-19249, 1983.

Mazzella, A., and H.F. Morrison, Electrical resistivity variations associated with earthquakes on the San Andreas fault, *Science, 185*, 855-857, 1974.

Morrow, C., and W.F. Brace, Electrical resisivity changes in tuffs due to stress, *J. Geophys. Res., 86*, 2929-2954, 1981.

Okada, Y., Internal deformation due to shear and tensile faults in a half space, *Bull. Seis. Soc. Am., 82*, 1018-1040, 1992.

Park, S. K., Monitoring resistivity changes prior to earthquakes in Parkfield, California with telluric arrays, *J. Geophys. Res.*, 96, 14211-14237, 1991.

Park, S.K., Monitoring resistivity changes in Parkfield, California: 1988-1995, *J. Geophys. Res., 102*, 24545-24559, 1997.

Park, S.K., Perspectives on monitoring resistivity changes with telluric signals at Parkfield, California: 1988-1999, *J. Geodynamics, 33*, 379-399, 2002.

Park, S.K., G.P. Biasi, R.L. Mackie, and T.R. Madden, Magnetotelluric evidence of crustal suture zones bounding the southern Great Valley, California, *J. Geophys. Res., 96*, 353-376, 1991.

Park, S.K., and D.V. Fitterman, Sensitivity of the telluric monitoring array in Parkfield, California to changes of resistivity, *J. Geophys. Res., 95*, 15,557-15,571, 1990.

Poll, H.E, J.T. Weaver, and A.G. Jones, Calculations of voltages for magnetotelluric modeling of a region with near-surface inhomogeneities, *Phys. Earth and Planet. Int., 53*, 287-297, 1989.

Prodehl, C. Crustal structure of the western United States, *U.S. Geol. Surv. Prof. Pap., 1034*, 74 pp., 1979.

Qian, F., Y. Zhao, M. Yu, Z. Wang, X. Liu, and S. Chang, Geoelectric resistivity anomalies before earthquakes, *Sci. Sinica, 26*, 326-336, 1983.

Roeloffs, E.A., and J. Langbein, The earthquake prediction experiment at Parkfield, California, *Rev. Geophys., 32*, 315-336, 1994.

Tank, S.B., Y. Honkura, Y. Ogawa, M. Matsushima, N. Oshiman, M.K. Tunçer, C. Çelik, E. Tolaf, and E.M. Işikara, Magnetotelluric imaging of the fault rupture area of the 1999 Izmit (Turkey) earthquake, *Phys. Earth Planet. Int., 150*, 231-225, 2005.

Unsworth, M., P. Bedrosian, M. Eisel, G. Egbert, and W. Siripunvaraporn, Along strike variations in the electrical structure of the San Andreas fault at Parkfield, California, *Geophys. Res. Lett., 27*, 3021-3024, 2000.

Unsworth, M.J., P.E. Malin, G.D. Egbert, and J.R. Booker, Internal structure of the San Andreas fault at Parkfield, California, *Geol., 25*, 359-362, 1997.

Unsworth, M. and P.A. Bedrosian, Electrical resistivity structure at the SAFOD site from magnetotelluric exploration, *Geophys. Res. Lett., 31*, doi10.1029/2003GL019405, 2004.

Yamazaki, Y., Electrical conductivity of strained rocks. The fourth paper. Improvement of the resistivity variometer, *Eq. Res. Inst. Bull., 46*, 957-964, 1968.

Yamazaki, Y., Coseismic resistivity steps, *Tectonophys., 22*, 159-171, 1974.

Zoback, M.D., and C.M. Wentworth, Crustal studies in central California using an 800 channel seismic reflection recording system, in *Reflection Seismology: A Global Perspective, Geodyn. Ser. vol. 13*, ed. by M. Barazangi and L. Brown, pp. 183-196, Amer. Geophys. Union, Washington, D.C., 1986.

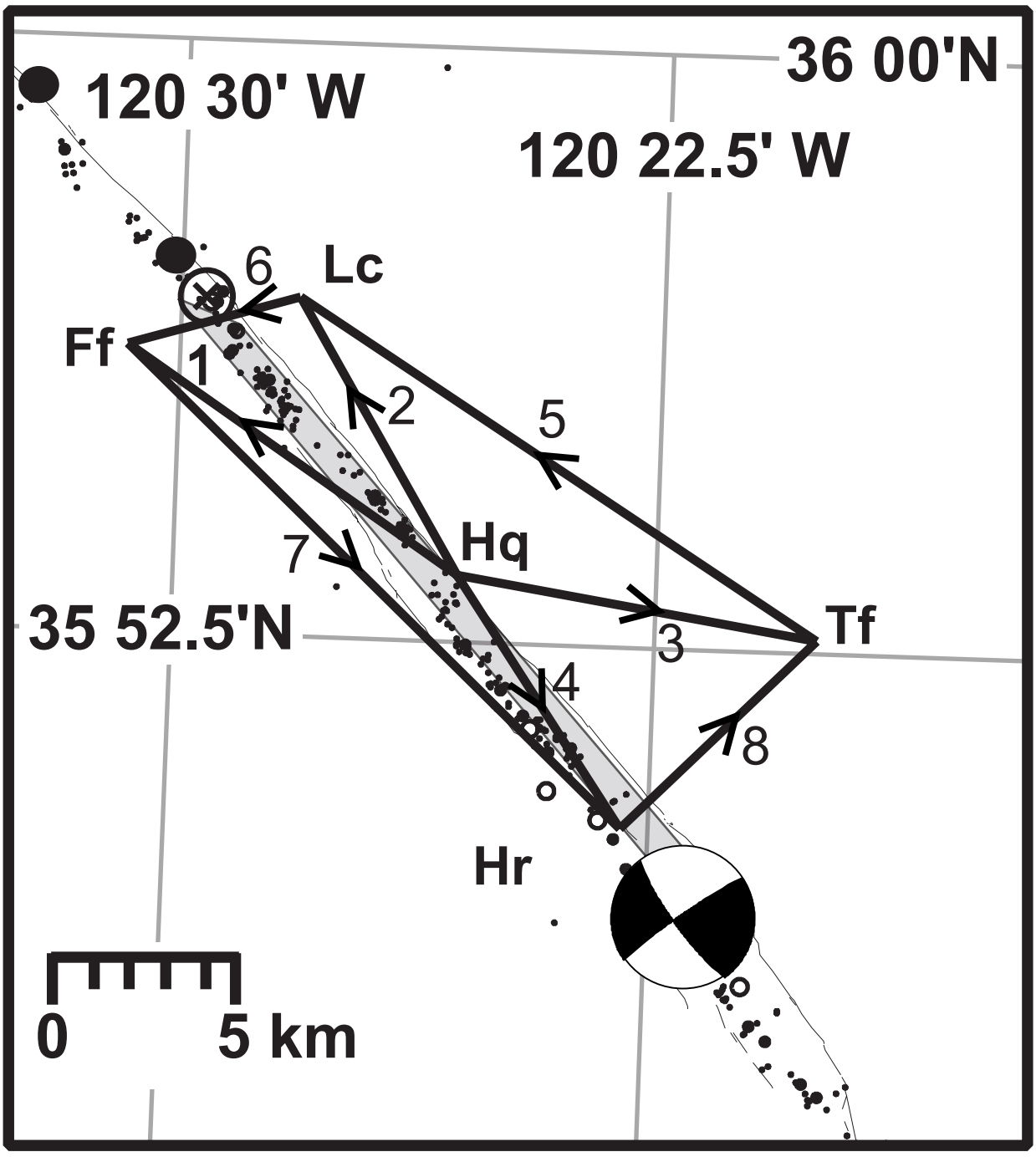

Fig 1

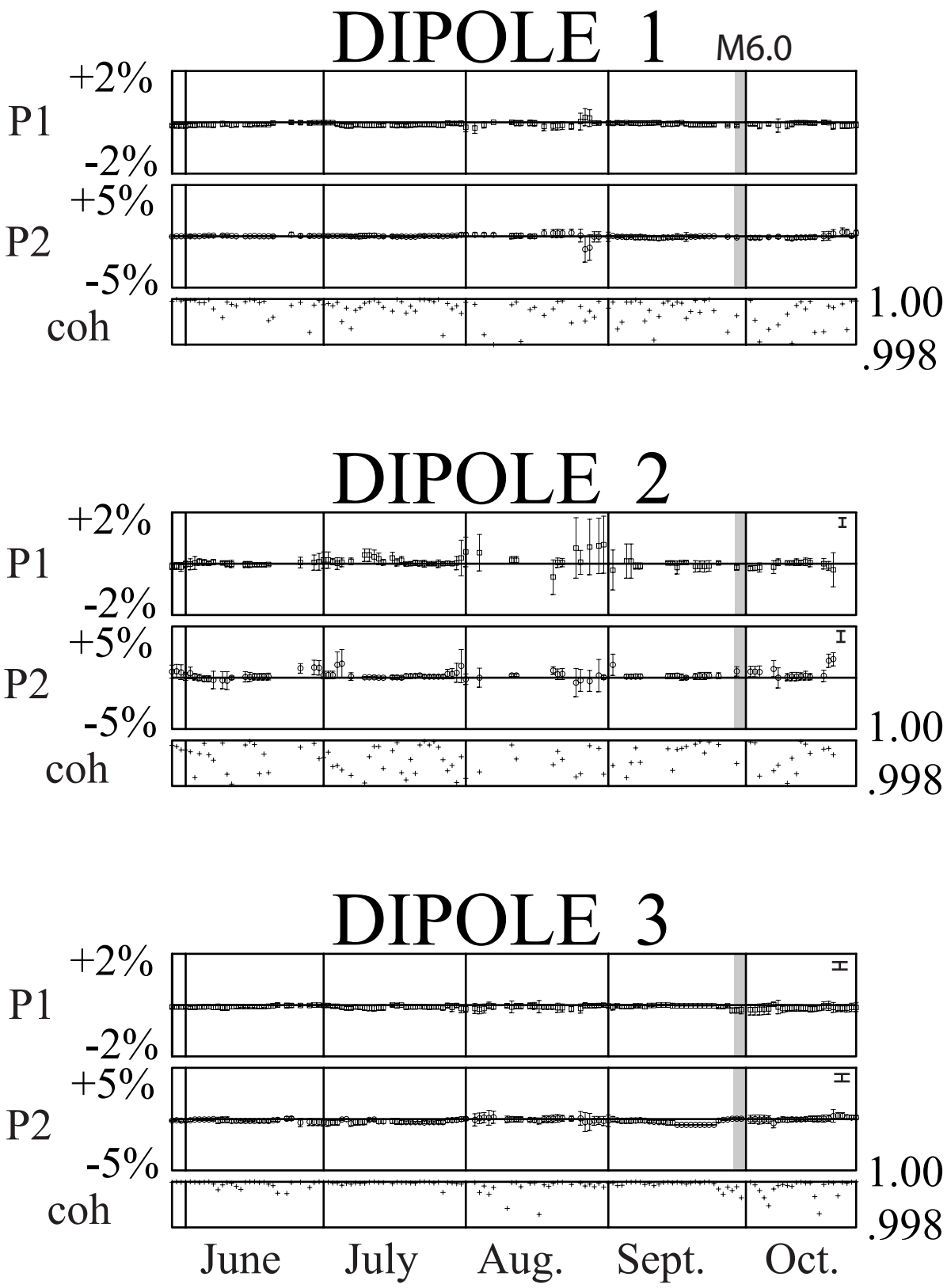
DIPOLE 1
M6.0
+2%
P1
-2%
+5%
P2
-5%
coh
1.00
.998
DIPOLE 2
+2%
P1
-2%
+5%
P2
-5%
coh
1.00
.998
DIPOLE 3
+2%
P1
-2%
+5%
P2
-5%
coh
1.00
.998
June
July
Aug.
Sept.
Oct.

Fig 2

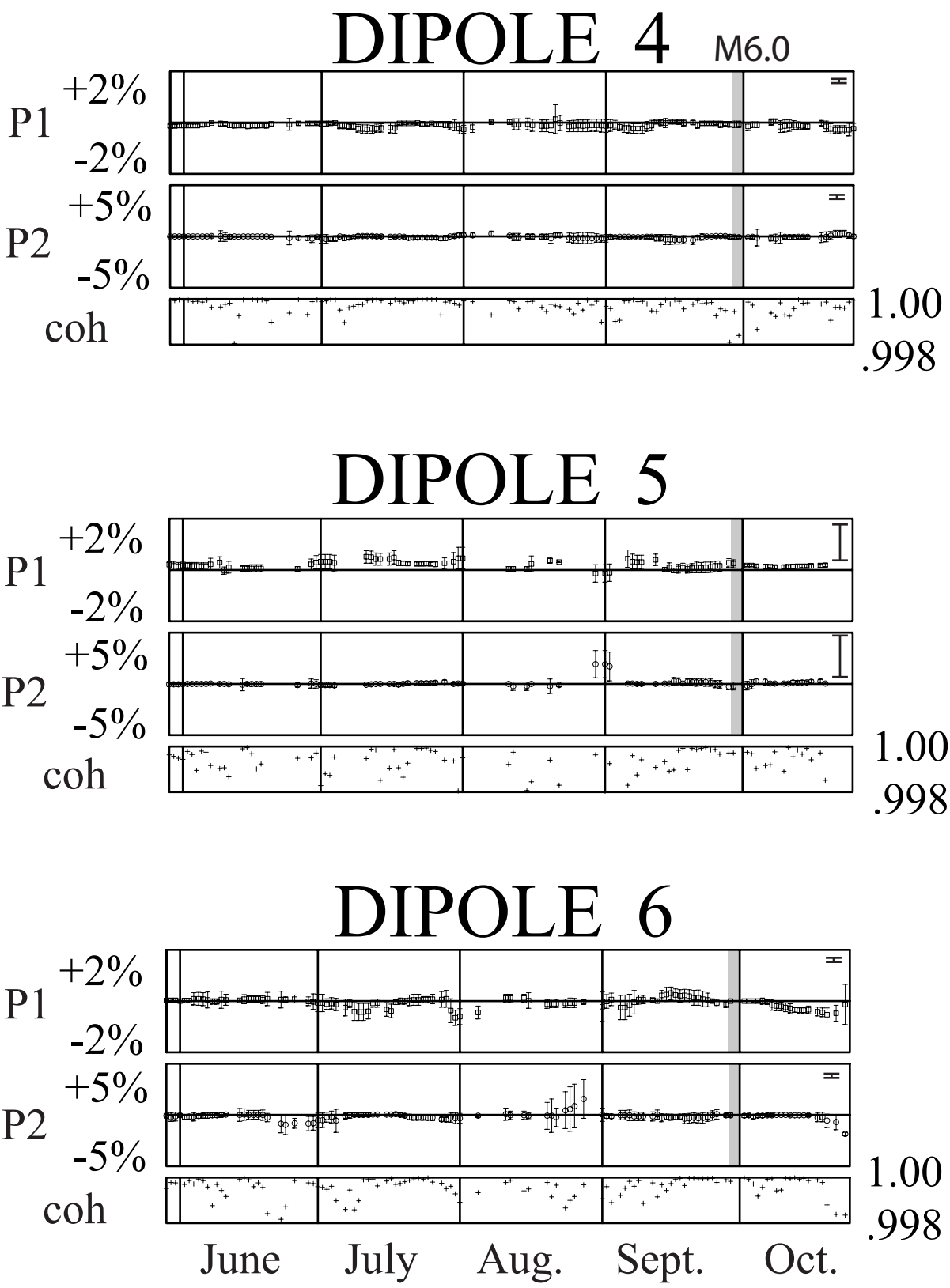
DIPOLE 4
M6.0
P1
+2%
-2%
P2
+5%
-5%
coh
1.00
.998
DIPOLE 5
P1
+2%
-2%
P2
+5%
-5%
coh
1.00
.998
DIPOLE 6
P1
+2%
-2%
P2
+5%
-5%
coh
1.00
.998
June
July
Aug.
Sept.
Oct.

Fig 3

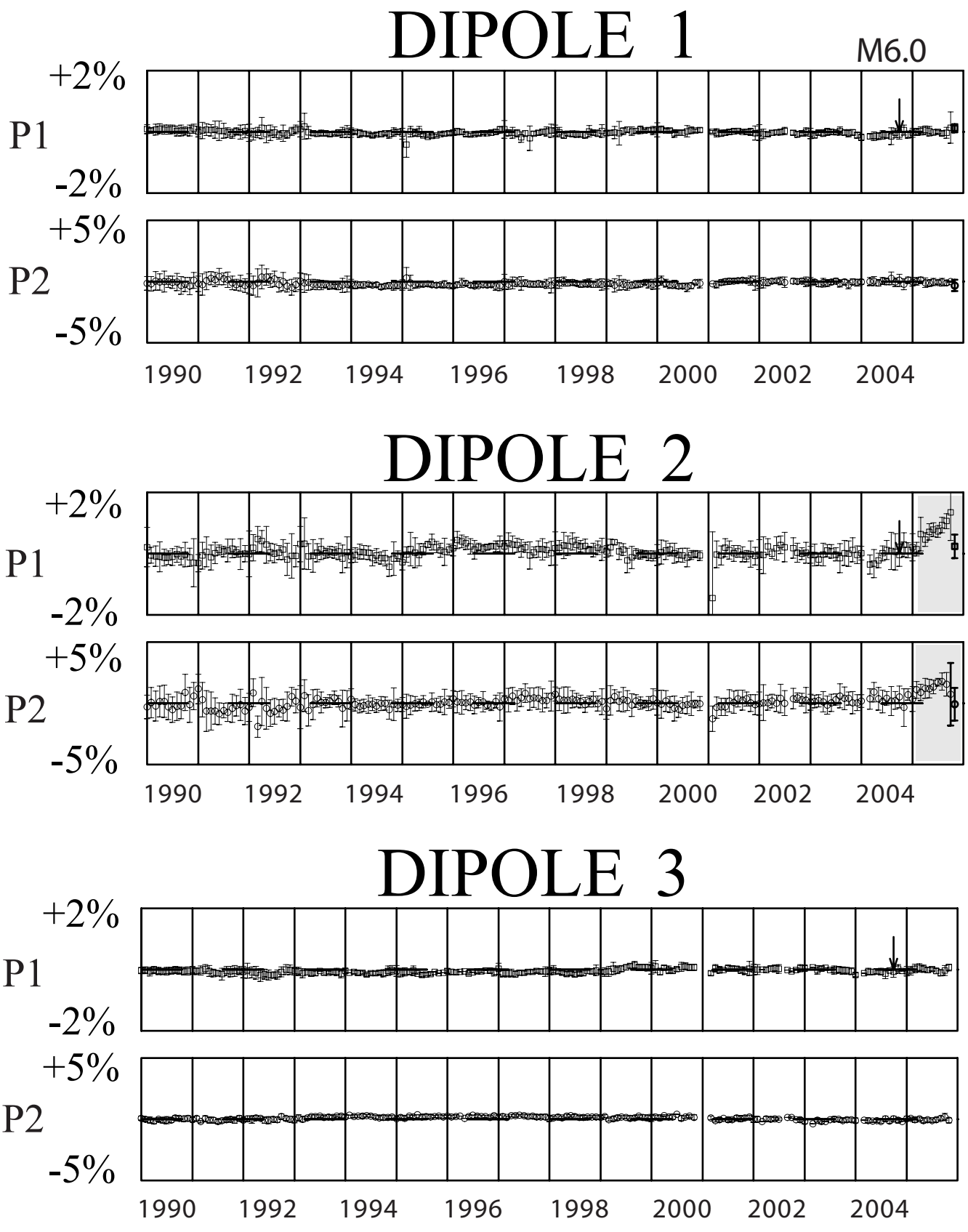
DIPOLE 1
M6.0
+2%
P1
-2%
+5%
P2
-5%
1990
1992
1994
1996
1998
2000
2002
2004
DIPOLE 2
+2%
P1
-2%
+5%
P2
-5%
1990
1992
1994
1996
1998
2000
2002
2004
DIPOLE 3
+2%
P1
-2%
+5%
P2
-5%
1990
1992
1994
1996
1998
2000
2002
2004

Fig 4

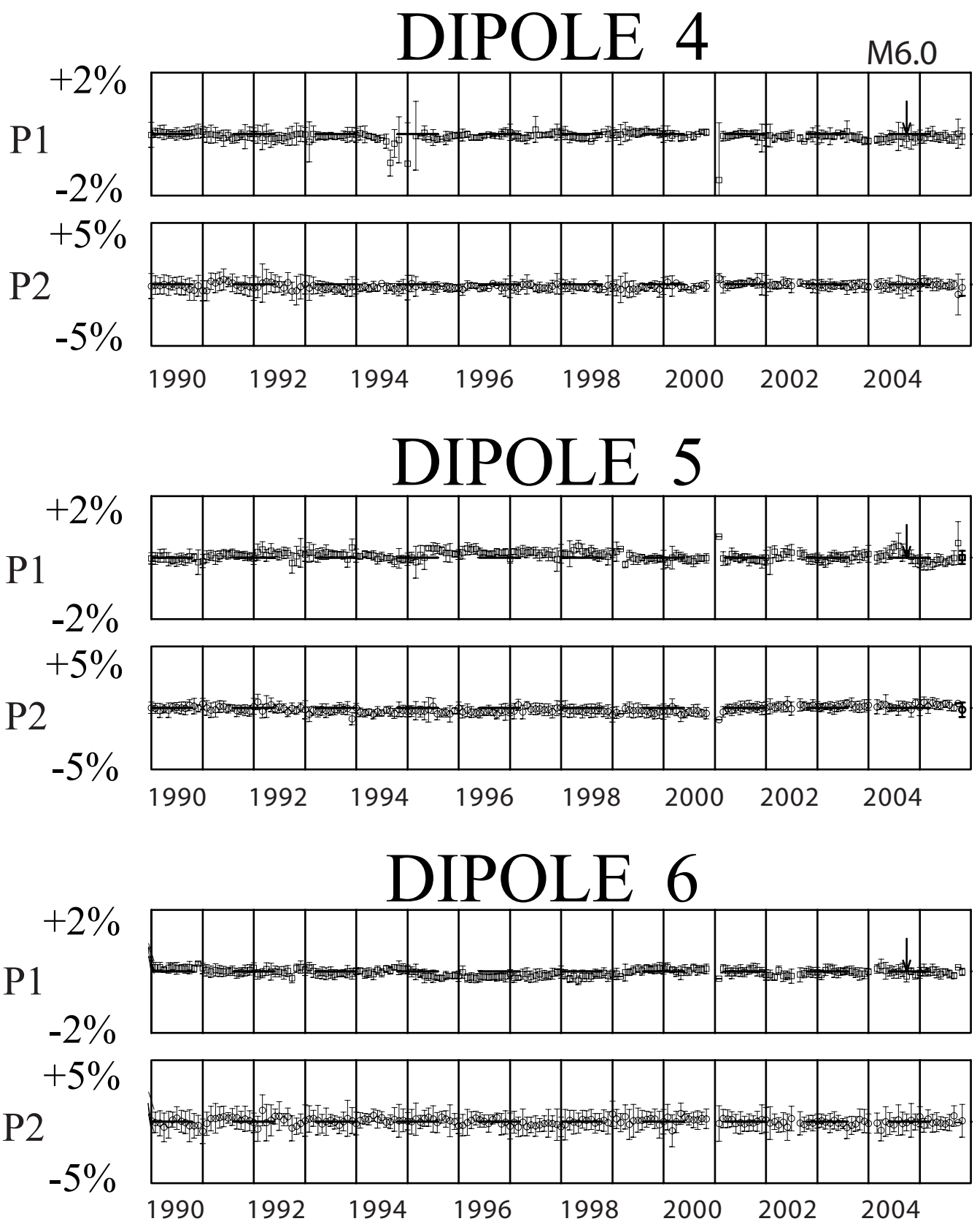
DIPOLE 4
M6.0
+2%
P1
-2%
+5%
P2
-5%
1990
1992
1994
1996
1998
2000
2002
2004
DIPOLE 5
+2%
P1
-2%
+5%
P2
-5%
1990
1992
1994
1996
1998
2000
2002
2004
DIPOLE 6
+2%
P1
-2%
+5%
P2
-5%
1990
1992
1994
1996
1998
2000
2002
2004

Fig 5

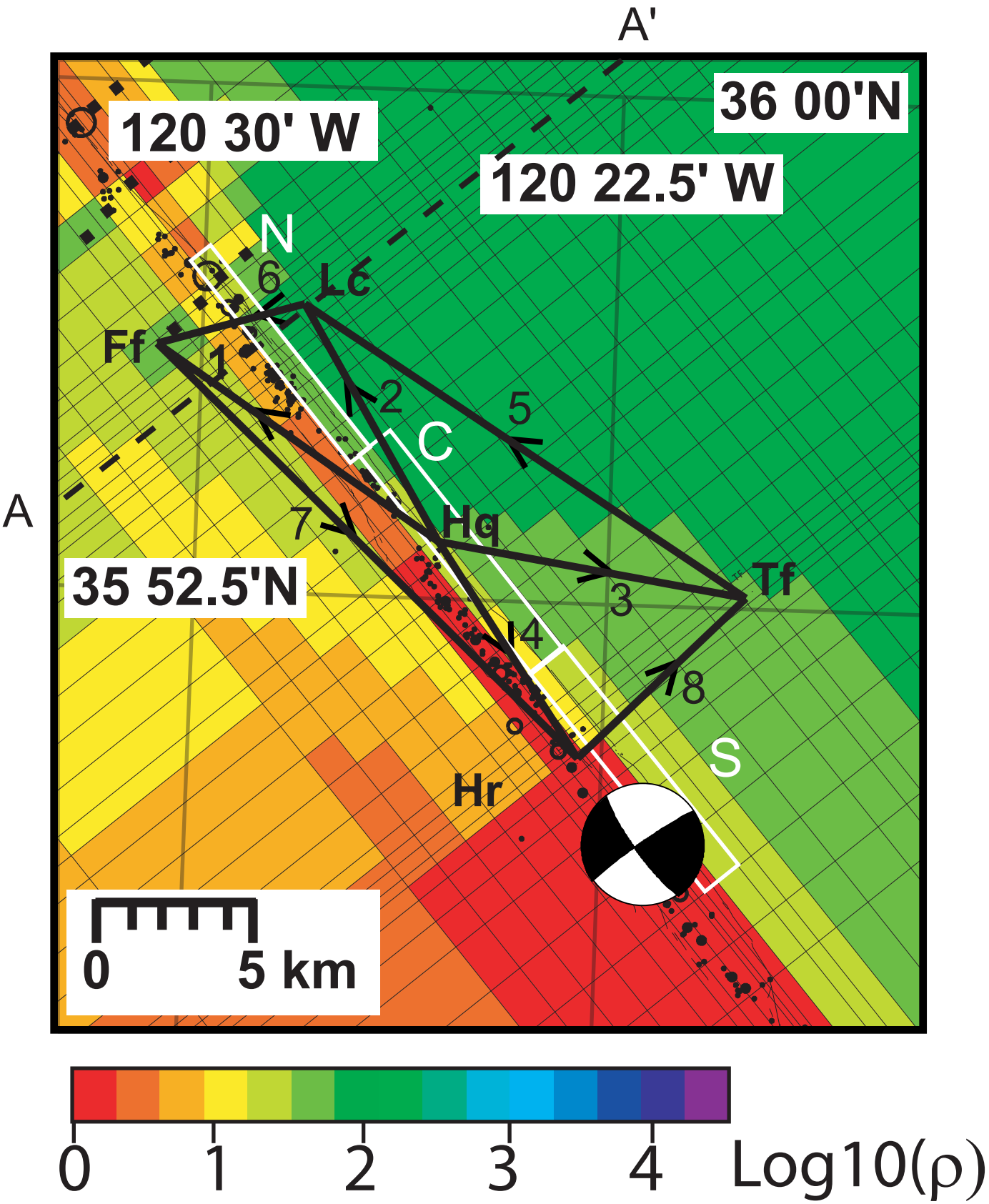
A'
A
120 30' W
120 22.5' W
36 00'N
35 52.5'N
N
Lc
Ff
C
Hq
Tf
S
Hr
1
2
3
4
5
6
7
8
0
5 km
0
1
2
3
4
Log10(ρ)

Fig 6A

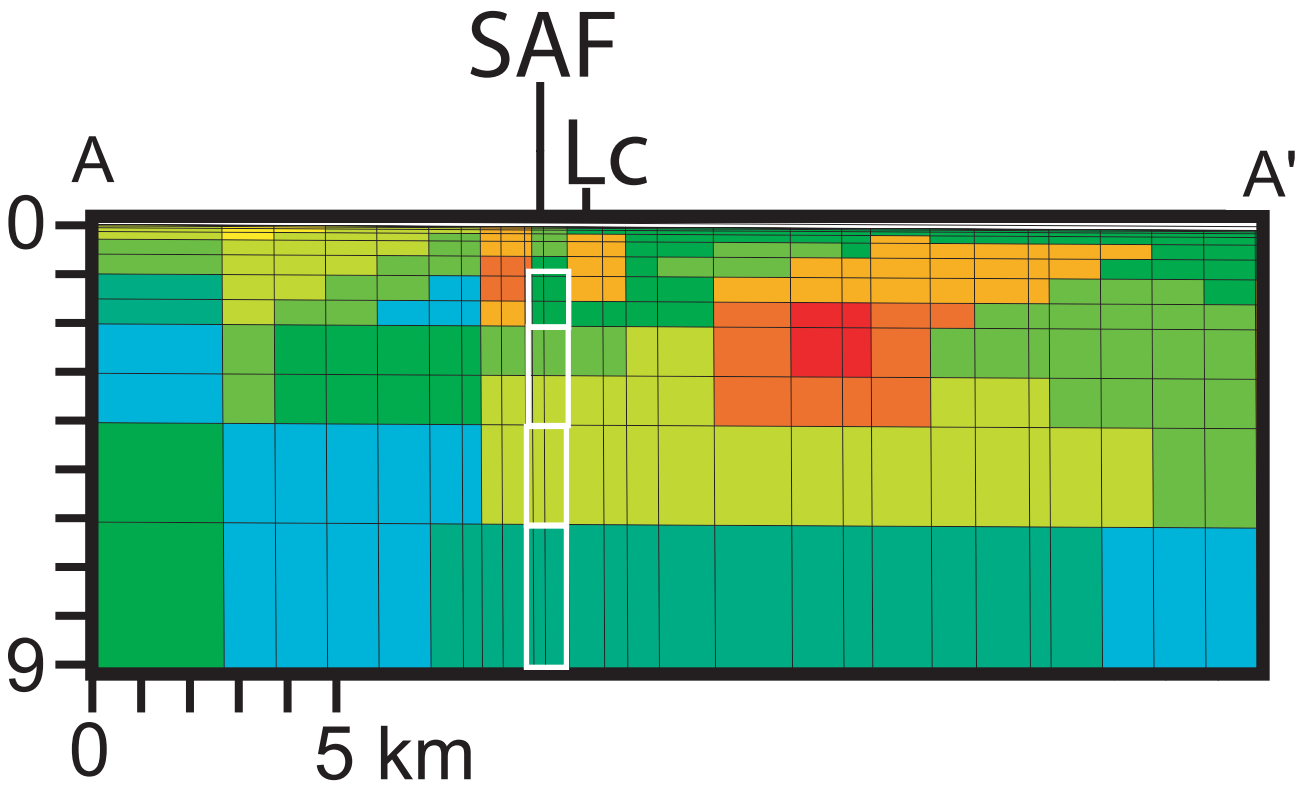

Fig 6b

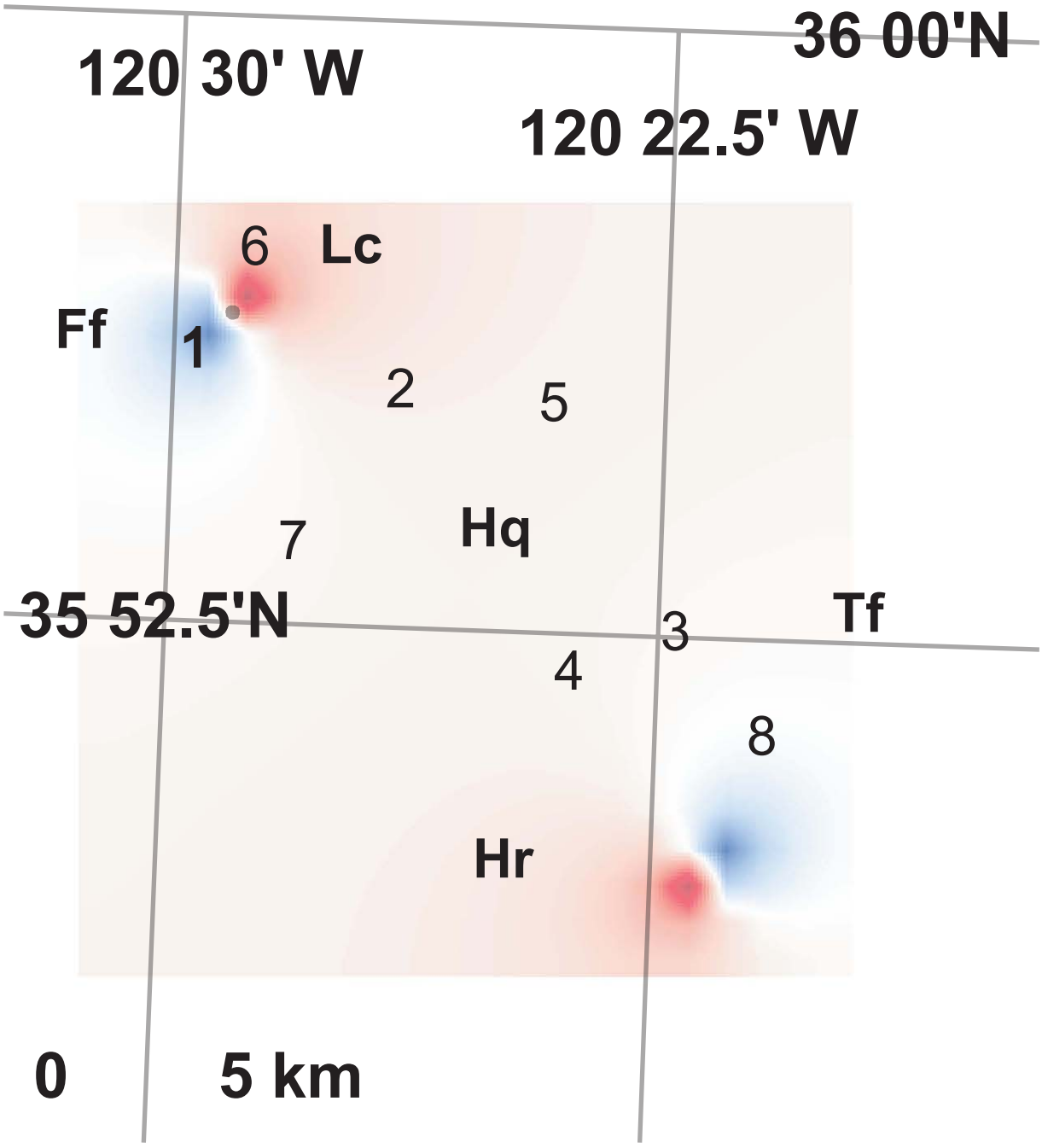
36 00'N
120 30' W
120 22.5' W
6
Lc
Ff
1
2
5
7
Hq
35 52.5'N
Tf
3
4
8
Hr
0
5 km
5.0
2.5
0
-2.5
-5.0
Δρ/ρ, %
-50
-25
0
25
50
Dilatation, με

Fig 7

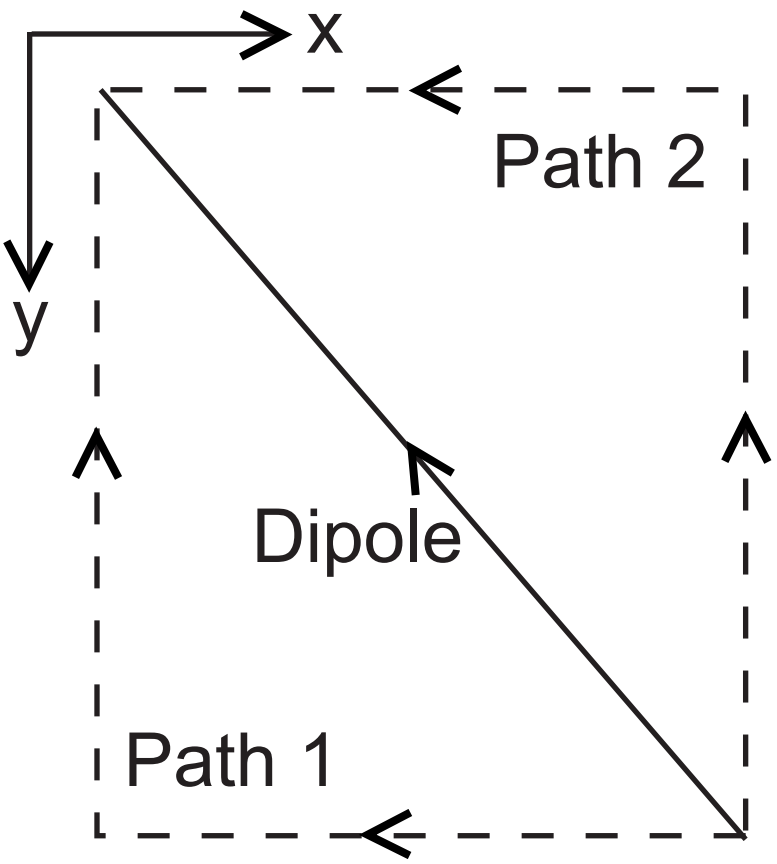

Fig A1